International Journal of Mechanical, Industrial and Aerospace Sciences
ISSN: 2517-9950
Vol:5, No:2, 2011

Unsteady Transonic Aerodynamic Analysis for Oscillatory Airfoils using Time Spectral Method

Mohamad Reza. Mohaghegh and Majid. Malek Jafarian

***Abstract*—**This research proposes an algorithm for the simulation of time-periodic unsteady problems via the solution unsteady Euler and Navier-Stokes equations. This algorithm which is called Time Spectral method uses a Fourier representation in time and hence solve for the periodic state directly without resolving transients (which consume most of the resources in a time-accurate scheme). Mathematical tools used here are discrete Fourier transformations. It has shown tremendous potential for reducing the computational cost compared to conventional time-accurate methods, by enforcing periodicity and using Fourier representation in time, leading to spectral accuracy. The accuracy and efficiency of this technique is verified by Euler and Navier-Stokes calculations for pitching airfoils. Because of flow turbulence nature, Baldwin-Lomax turbulence model has been used at viscous flow analysis. The results presented by the Time Spectral method are compared with experimental data. It has shown tremendous potential for reducing the computational cost compared to the conventional time-accurate methods, by enforcing periodicity and using Fourier representation in time, leading to spectral accuracy, because results verify the small number of time intervals per pitching cycle required to capture the flow physics.

***Keywords*—**Time Spectral Method, Time-periodic unsteady flow, Discrete Fourier transform, Pitching airfoil, Turbulence flow

I. Introduction

UNSTEADY flow calculations have been used extensively including in the flutter analysis, analysis of flow around helicopter blades and etc. In these matters, flow behavior is often unsteady but periodic.

In analyzing these problems using algorithms that can use the periodic property of flow can be useful. Traditional time stepping methods do not consider this property. Explicit schemes for stability use small time steps that this is time-consuming. Implicit schemes, although use a larger range of time step, but because the long repeat process to achieve solution convergence, these schemes are expensive especially for three-dimensional problems. Time accurate solvers like the implicit second-order Backward Difference Formula (BDF) requires Integration on several periods with small time steps to achieve periodic steady state. It takes a long time.

What is important in the numerical solution is the balance between computation time and accuracy of solution. On traditional schemes, some method, such as adaptive grid methods because of limited time steps, are inherently time consuming and on other schemes like BDF, if time steps are chosen large, accurate solution comes down, and when the time steps are small, time resolved intensity will increase. Therefore, an algorithm is suitable also reduce the time to solve also maintain good accuracy.

In recent years, researchers have turned to using Fourier-based algorithms to significantly reduce the computational expense for analyzing unsteady periodic problems.

Hall et al. [1] did the first study in this field. He introduced the harmonic balance method for solving nonlinear equations in frequency space. Subsequently, McMullen et al. [2] introduced non-linear frequency domain (NLFD) method. In this method, firstly equations are converted to frequency space and then solved in frequency space, the flow variables are returned into the physical space. From where the method is required fast Fourier transform (FFT) and inverse fast Fourier transform (IFFT), so to use this method, it is required substantial changes in existent flow solvers. Subsequently, Gopinath and Jameson [3] proposed using a Fourier collocation matrix for the temporal derivative term and time integration to prevent FFT, IFFT and the use of minimal changes in the time accurate flow solver. This scheme is called Time Spectral method. In this method, time derivative term couple all the time levels in the period through Fourier collocation matrix. Unlike finite difference methods that use only several of the term of solution variable to calculate the derivative term, Time Spectral method uses all the time levels in the period, in the derivative term calculation, thus has very high accuracy. Here, unlike time marching methods, have been solved the flow variables simultaneously at all time instances and this process repeat until to reach a periodic steady state. The detailed algorithm of this technique will be presented in next section.

In this paper Time Spectral method has been used for simulation of 2D external aerodynamics test cases as pitching airfoils. These test cases are NACA 64A010 test case 6 (CT6) with small oscillation amplitude and weak shock waves and NACA 0012 test case 5 (CT5) with large oscillation amplitude and strong shock waves. The results numerical are compared with experimental data. Two different airfoils, the NACA 64A010 and the NACA 0012, were tested by Davis [4] and Landon [5] respectively. The experimental data was published as part of AGARD report 702.

M.S.C of Department of Mechanical Engineering, Birjand University, Birjand 97175-615, Iran. Email: mor.mohaghegh@gmail.com.
Assistant Professor of Department of Mechanical Engineering, Birjand University, Birjand 97175-615, Iran. Email: mmjafarian@excite.com.

II. Governing Equations

The compressible flow around a pitching airfoil is physical problem that study in this research. Generally compressible flows are simulated by Navier-Stokes equation.

A. Conservative Form of the Field Equations

The two-dimensional conservative form of the Navier-Stokes equation in Cartesian coordinates is:

$$\frac{\partial(\forall w)}{\partial t}+\frac{\partial f}{\partial x}+\frac{\partial g}{\partial y}=\frac{\partial f_v}{\partial x}+\frac{\partial g_v}{\partial y} \tag{1}$$

Where the state vector w, inviscid flux vector f and g and viscous flux vector f_v and g_v are described respectively by:

$$w=\begin{bmatrix}\rho\\ \rho u\\ \rho v\\ \rho e\end{bmatrix} \tag{2}$$

$$f=\begin{bmatrix}\rho(u-x_t)\\ \rho u(u-x_t)+p\\ \rho v(u-x_t)\\ \rho e(u-x_t)+pu\end{bmatrix}, g=\begin{bmatrix}\rho(v-y_t)\\ \rho u(v-y_t)\\ \rho v(v-y_t)+p\\ \rho e(v-y_t)+pv\end{bmatrix} \tag{3}$$

$$f_\upsilon=\begin{bmatrix}0\\ \tau_{xx}\\ \tau_{xy}\\ u\tau_{xx}+v\tau_{xy}-q_x\end{bmatrix}, g_\upsilon=\begin{bmatrix}0\\ \tau_{xx}\\ \tau_{xy}\\ u\tau_{xx}+v\tau_{xy}-q_x\end{bmatrix} \tag{4}$$

Where ρ is the density, u and v are component velocity at x and y directions respectively, x_t and y_t are component velocity of grid, p is pressure and e is the total energy per unit mass. As, temperature T and total energy e are determined by the ideal gas equation of state:

$$e=\frac{p}{\rho(\gamma-1)}+\frac{1}{2}(u^2+v^2) \tag{6}$$

$$T=\frac{p}{\rho R} \tag{7}$$

Where R is the gas constant. Suppose cell volume $\forall$ does not vary in time, then semi-discrete form of the unsteady equations in Cartesian coordinates can be written as follow:

$$\forall\frac{\partial w}{\partial t}+R(w)=0 \tag{8}$$

Where

$$R(w)=\frac{\partial f_i}{\partial x_i} \tag{9}$$

B. The Time Spectral Method

The core of this method is based on discrete Fourier transform for solving periodic unsteady partial differential equations. The discrete Fourier transform of w, for a time period T, is given by

$$\hat{w}_k=\frac{1}{N}\sum_{n=0}^{N-1}w^n e^{-ik\frac{2\pi}{T}n\Delta t} \tag{10}$$

And its inverse transform,

$$w^n=\begin{cases}\sum_{k=-\frac{N}{2}}^{\frac{N}{2}-1}\hat{w}_k e^{ik\frac{2\pi}{T}n\Delta t} & : \text{N is even}\\ \sum_{k=-\frac{N-1}{2}}^{\frac{N-1}{2}}\hat{w}_k e^{ik\frac{2\pi}{T}n\Delta t} & : \text{N is odd}\end{cases} \tag{11}$$

Where the time period T is divided into N time intervals, Δt=T/N.

The Fourier transform of the derivative approximations at nth time interval is computed by (see appendix A):

$$D_t w^n=\frac{2\pi}{T}\sum_{j=0}^{N-1}d_n^j w^j \tag{12}$$

Where d_n^j is defined by

$$d_n^{j\,even}=\begin{cases}\frac{1}{2}(-1)^{n-j}\cot(\frac{\pi(n-j)}{N}) & : n\neq j\\ 0 & : n=j\end{cases} \tag{13}$$

And

$$d_n^{j\,odd}=\begin{cases}\frac{1}{2}(-1)^{n-j}\operatorname{cosec}(\frac{\pi(n-j)}{N}) & : n\neq j\\ 0 & : n=j\end{cases} \tag{14}$$

Since flow is periodic in time here, so the state vector w periodic in time, too. Therefore, its derivative can be expressed using (13).Using (2.6), the governing equations in semi-discrete form are:

$$\forall D_t w^n+R(w^n)=0 \tag{15}$$

Introducing pseudo time, τ, to (2.13) in the same manner as the implicit dual time stepping scheme,

$$\forall\frac{dw^n}{d\tau}+\forall D_t w^n+R(w^n)=0 \tag{16}$$

The solver used for this purpose is a conservative cell-centered finite volume scheme. A local time stepping is used for accelerating convergence, in which a pseudo-time step with a five-stage Runge-Kutta scheme is performed at each level. The Jameson-Schmidt-Turkel (JST) [6] scheme is used as the artificial dissipation scheme where blended first and third order dissipation terms are introduced to suppress spurious modes and ensure stability.

C. Baldwin-Lomax Turbulence Model

The Baldwin and Lomax [7] turbulence model is an algebraic model for the determination of the eddy viscosity. μ_{turb} as a function of the local boundary layer velocity profile. The model is suitable for high-speed flows with thin attached boundary-layers, typically present in aerospace and turbomachinery applications. It is commonly used in quick design iterations where robustness is more important than capturing all details of the flow physics. The dual layered eddy viscosity formulation is sufficient to complete the Reynolds Averaged Navier-Stokes equation. The turbulent eddy viscosity coefficient can be calculated as

$$\frac{\mu_{turb}}{\mu_{\infty}} = \begin{cases} \mu_{turb_{inner}} , where\ y < y_{crossover} \\ \mu_{turb_{outer}} , where\ y > y_{crossover} \end{cases} \quad (17)$$

Where $y_{crossover}$ is the minimum value of the dimensionless normal distance to the wall, $y_{crossover}$ at which the inner and outer eddy viscosity formulations produce the same result. Finally, after μ_{turb} calculation (see Baldwin and Lomax [7]), viscosity of flow will be defined as

$$\mu = \mu_{lam} + \mu_{turb} \quad (18)$$

Where μ_{lam} is laminar flow viscosity that is defined by Sutherland equation defined as

$$\mu_{lam} = \frac{(1.458 \times 10^{-6}) T^{\frac{3}{2}}}{T + 110.4} \quad (19)$$

III. Numerical Results and Discussions

This section presents the results of simulations using both the Euler and the Reynolds averaged Navier-Stokes equations using a Baldwin-Lomax turbulence model.

A. Test Cases

The Pitching airfoils are ample ground for validating the algorithm with experimental and other established numerical results.This research uses two different test cases, NACA 0012 airfoil (CT5) and 64A010 airfoil (CT6). The important parameters used in the description of these cases are summarized in Table 1 [4], [5].

TABLE I
Characteristics of the Pitching Airfoil Test Cases

Description	Variable	Davis Experiment	Landon Experiment
AGARD Case Number		CT6	CT5
Airfoil		NACA 64A010	NACA 0012
Mean Angle of Attack	α_m	0.0°	0.016°
Angle of Attack Variation	α_0	±1.01°	±2.51°
Reynolds Number	Re_{∞}	12.56×10^6	5.5×10^6
Mach Number	M_{∞}	0.796	0.755
Reduced Frequency	k_c	0.202	0.0814
Pitching Axis	x_m	24.8	25

The sinusoidal pitching motion of the airfoil is given in terms of the variation of angle of attack as a function of time,

$$\alpha(t) = \alpha_m + \alpha_0 \sin(\omega t) \quad (20)$$

Where α_m is the mean angle of attack, α_0 is the maximum pitching amplitude with respect to the mean, and ω the angular velocity, is expressed in terms of a non dimensional parameter, the reduced frequency, k_c the reduced frequency is defined as

$$k_c = \frac{\omega l_c}{2U_{\infty}} \quad (21)$$

Here l_c, the characteristic length is the root chord length. The data for the 64A010 airfoil is for a transonic symmetric airfoil oscillating at a low reduced frequency over a limited range in angle of attack. Because of this fairly small variation in angle of attack, the numerical results are considered to be less sensitive to the choice of turbulence model than the data for the 0012 airfoil. Another factor contributing to its selection was its popularity in the numerical analysis community. Numerous existing numerical results are available for comparison with those produced by the Time Spectral method. In comparison to the data for the 64A010, the data for the 0012 was obtained at a lower Reynolds number but with an angle of attack variation approaching the stall boundary. The increased sensitivity of these results to the choice of turbulence model is a drawback. Therefore viscous results are represented only for NACA0012 test case.

B. Computational Grid

The first step in numerical discretization is to represent the continuous domain by a mesh of discrete points, where the dependent variables of the governing equation are

represented. Mesh generation has become an important field of study to enable solutions for more complex geometries. The choice of the type of mesh is usually based on the complexity of the geometry and the desired level of accuracy and approximation of the continuous problem.In NACA 64A010 results section , where only the Euler equations are employed, large gradients close to the surface of the airfoil except for the shock wave do not exist and more uniform and regular meshes are sufficient to provide accurate numerical approximations (Fig. 1.(a)). However, in NACA 0012 results section where the Navier-Stokes equations are used in the numerical simulation in a two-dimensional viscous flow environment, a high mesh resolution close to the surface of the airfoil is required to resolve the boundary layer and its interaction with the shock wave (Fig. 1.(c)).

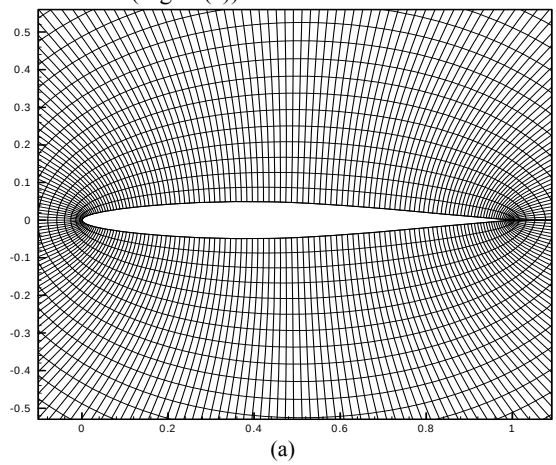

(a)

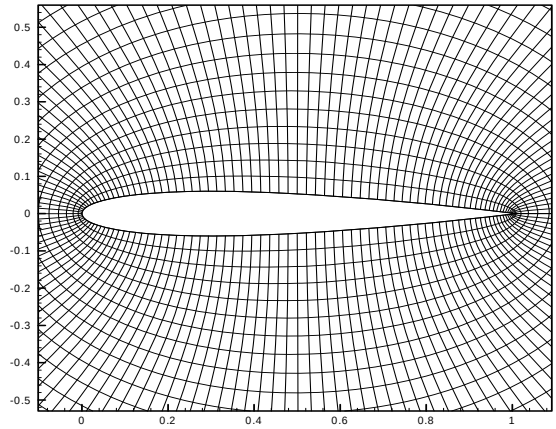

(b)

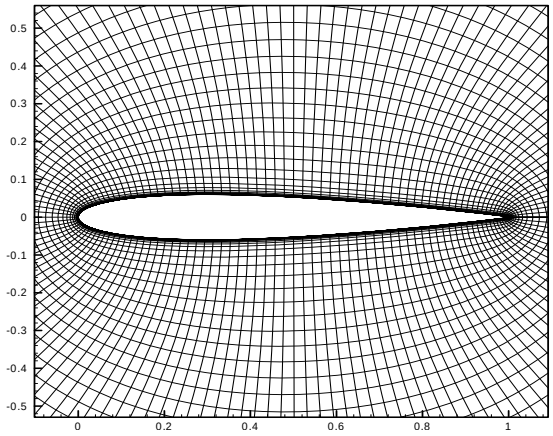

(c)

Fig. Nearfield resolution of O-mesh grids. (a) 271x61 points used in the Euler calculations for NACA 64A010 (b) 149x51 points used in the Euler calculations for NACA 0012 (c) 149x51 points used in the unsteady Navier-Stokes calculations for NACA 0012

C. Inviscid results for NACA 64A010 airfoil

C.1 Coefficient of Pressure Results

Fig. 2 (a) to (d) show both the numerical and experimental Cp results along the airfoil at any quarter of period, phase 0.0°, 90°, 180° and 270°. Very good agreement between Time Spectral and experimental results are evident.

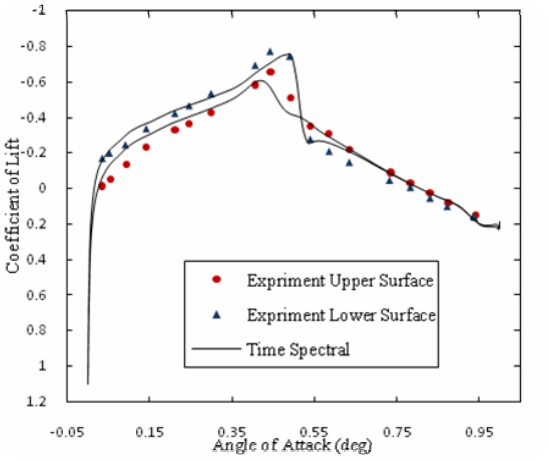

(a)

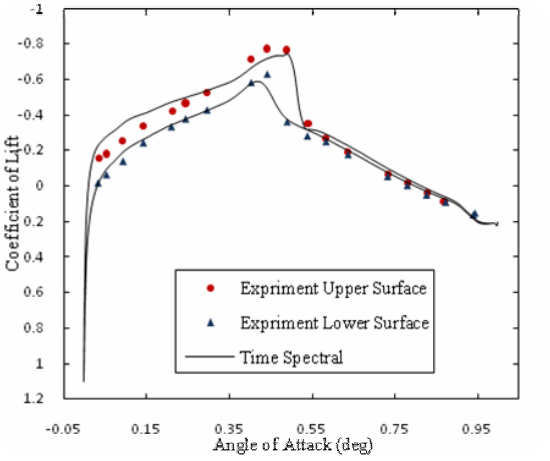

(b)

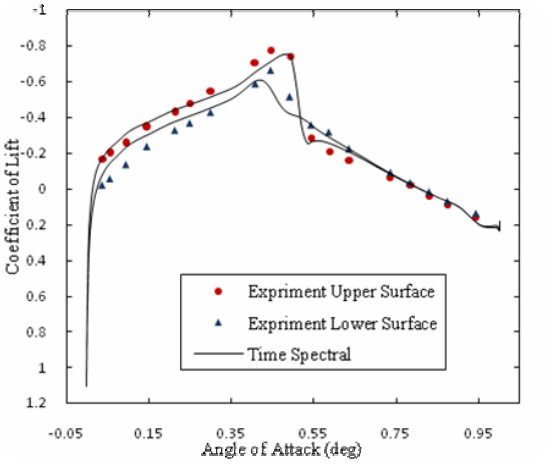

(c)

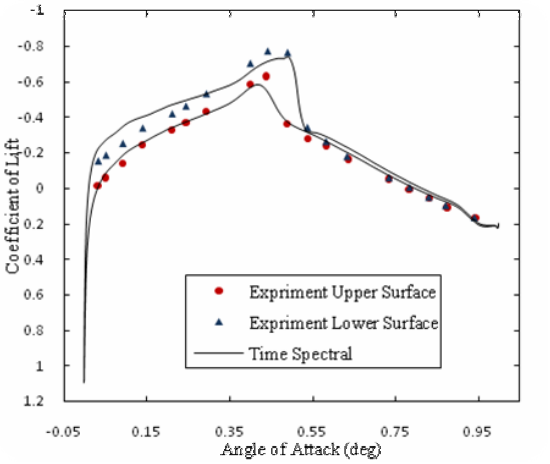

(d)

Fig. 2 Comparison of Cp data with experimental results for NACA 64A010 airfoil (a) $\alpha = 0$ upward, phase 0.0° (b) $\alpha = 1.01$ phase 90° (c) $\alpha = 0$ downward, phase 180° (d) $\alpha = -1.01$, phase 270°

Coefficient of Lift Results

Fig. 3 shows both the numerical and experimental *Cl* results as a function of the instantaneous angle of attack. A subfigure shows several ellipses each computed using a different number of time intervals. These plots show that the variation in time varying *Cl* as a function of the temporal resolution is negligible, and that results convergent to plotting accuracy can be obtained using only four time intervals.

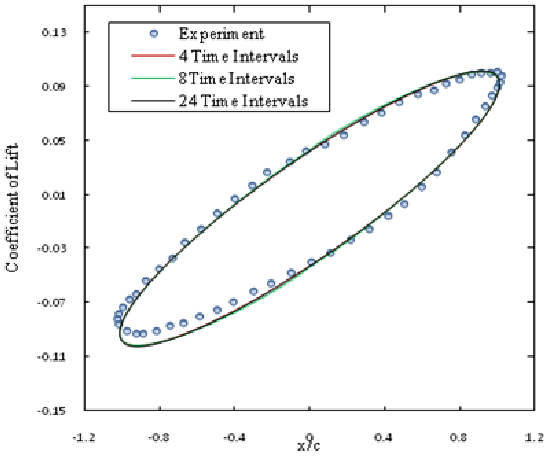

Fig. 3 Comparison of *Cl* data with Davis's 64A010 experiment

Instantaneous Pressure Distribution

Finally, Fig 4 (a) and Fig 4 (b) show instantaneous pressure distribution around pitching airfoil at equally spaced time levels for NACA 64A010 airfoil.

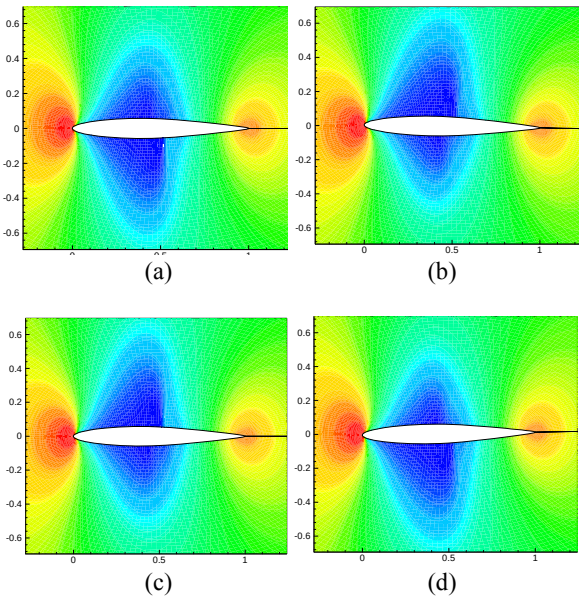

(a) (b)

(c) (d)

Fig. 4 Instantaneous pressure distribution around CT6 at equally spaced time levels

D.Inviscid and viscous results for NACA 0012 airfoil

Coefficient of Pressure Results

Fig 5 (a) and (b) show both the numerical and experimental Cp results along the NACA 0012 airfoil for inviscid and viscous flow at an angle of attack that experimental data were exist. With comparison Fig 5. (a) and (b) has been observed abrupt variation in Cp graphs that is produced due to shock wave, in viscous flow is smoother than inviscid flow because of boundary layer interaction with the shock wave.

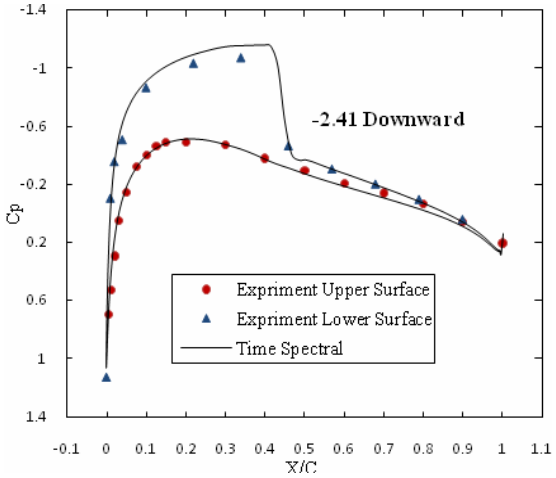

(a)

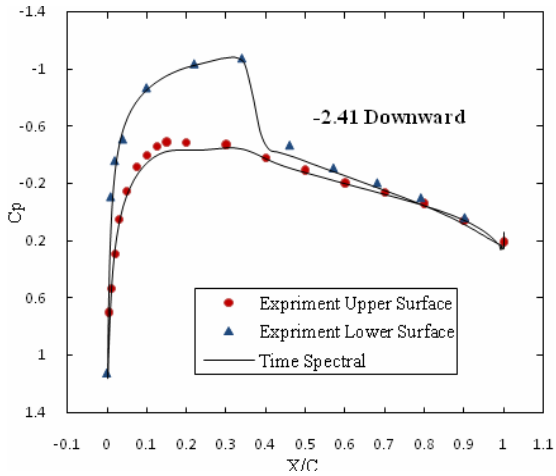

(b)

Fig. 5 Comparison of Cp data with experimental results for NACA 0012 airfoil. (a) Inviscid flow (b) Viscous flow

Coefficient of Lift Results

Figures 6 (a) and 6. (b) show both the numerical and experimental C_l results as a function of the instantaneous angle of attack for inviscid and viscous flow. In viscous results analysis, has been used Baldwin-Lomax turbulence model.

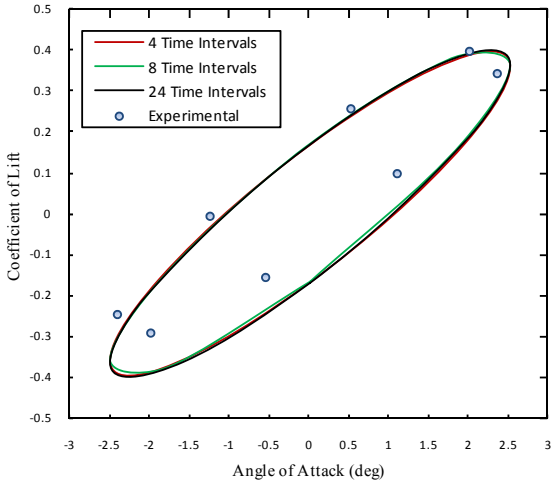

(a)

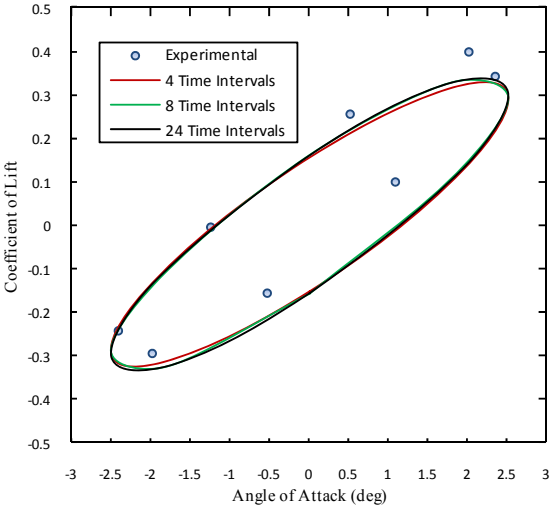

(b)

Fig. 6 Comparison of *Cl* data with experimental results for the AGARD CASE. (a) Inviscid flow (b) Viscous flow

Instantaneous Pressure Distribution

Finally, Fig 7. (a) and 7. (b) show instantaneous pressure distribution around pitching airfoil at maximum of pitch angle.

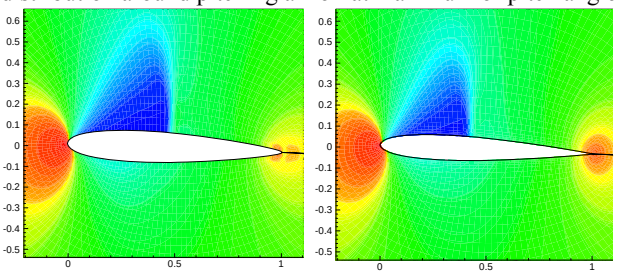

(a) (b)

Fig. 7 Instantaneous pressure distribution around CT5. (a) , inviscid flow (b) , viscous flow equally spaced time levels

So that has been alluded previously, because of boundary layer interaction with the shock wave in viscous flow, shock wave is weakly than inviscid flow. It has delineated by comparing Figures 7. (a) and 7. (b).

IV. Conclusions

The Time Spectral method is an intense method in Time-periodic unsteady flow analysis. So, that presents a proper accuracy of the solution and a low time for convergence. Conforming to a time accurate existing solver is other preference of this method. Time Spectral method performs all the calculations in the time domain, and hence requires minimal modifications to an existing solver. This algorithm which is simpler to implement than the typical NLFD type solver because it does not require the multiple operations of Fourier transforms and inverse Fourier transforms, while still achieving better convergence and reducing computational cost in comparison to the typical implicit schemes.

The Baldwin-Lomax model is suitable for high-speed flows with thin attached boundary-layers, typically present in aerospace and turbomachinery applications. The model is not suitable for cases with large separated regions and significant curvature/rotation effects.

Appendix A

A. Fourier Collocation Matrix

This section discusses details of compact representation of the spectral Fourier derivative operator in the physical space, instead of the wave space. The derivation is based on lecture notes of Moin [8].

Assume that f(x) is a function with a period of T defined on the grid,

$$x_j = \frac{Tj}{N} \quad \text{where} \quad j=0,1,2,...,N-1 \tag{1}$$

1) A.1 Even Formulation

The discrete Fourier transform of f(x) is given by

$$\hat{f}_k = \frac{1}{N}\sum_{n=0}^{N-1} f(x_j) e^{-ik\frac{2\pi}{T}x_j} \tag{A.1}$$

and its inverse transform given by

$$f(x_j) = \sum_{k=-\frac{N}{2}}^{\frac{N}{2}-1} \hat{f}_k e^{ik\frac{2\pi}{T}x_j}$$

The spectral derivative of f(x) at point j is given by

$$\left.\frac{df(x)}{dx}\right|_j = \frac{2\pi}{T}\sum_{k=-\frac{N}{2}+1}^{\frac{N}{2}-1} ik\hat{f}_k e^{ik\frac{2\pi}{T}x_j}$$

Substitute for $\hat{f}_k$ from equation (A.1), to obtain

$$\left.\frac{df(x)}{dx}\right|_n = \frac{1}{N}\frac{2\pi}{T}\sum_{k=-\frac{N}{2}+1}^{\frac{N}{2}-1}\sum_{j=0}^{N-1} ikf(x_j) e^{-ik\frac{2\pi}{T}x_j} e^{ik\frac{2\pi}{T}x_n}$$

Note that: $x_j = \frac{Tj}{N}$, $x_n = \frac{Tn}{N}$

$$Df\big|_n = \frac{1}{N}\frac{2\pi}{T}\sum_{k=-\frac{N}{2}+1}^{\frac{N}{2}-1}\sum_{j=0}^{N-1} ikf(x_j) e^{ik\frac{2\pi}{N}(n-j)}$$

Let:

$$d_n^j = \frac{1}{N}\frac{2\pi}{T}\sum_{k=-\frac{N}{2}+1}^{\frac{N}{2}-1} ike^{ik\frac{2\pi}{N}(n-j)} \tag{A.2}$$

Then

$$Df\big|_n = \frac{2\pi}{T}\sum_{j=0}^{N-1} d_n^j f(x_j)$$

Which is matrix-vector multiplication process where the elements of the matrix are d_n^j and the vector is $f(x_j)$. The elements d_n^j of the matrix can be computed analytically. First, the sum in equation (A.2) is computed. Let

$$s = \sum_{k=\frac{N}{2}+1}^{\frac{N}{2}-1} e^{ikx} = e^{i(-\frac{N}{2}+1)x} + e^{i(-\frac{N}{2}+2)x} + ... + e^{i(\frac{N}{2}-1)x}$$

Using the geometric series, the summation can be evaluated as,

$$s = e^{i(-\frac{N}{2}+1)x}\left[1 + e^{ix} + e^{2ix} + ... + e^{i(N-2)x}\right] = e^{i(-\frac{N}{2}+1)x}\frac{1-e^{i(N-1)x}}{1-e^{ix}} \tag{A.3}$$

Multiplying numerator and Denominator in equation (A.3) by $e^{-i\frac{x}{2}}$ term, to obtain

$$S = \frac{e^{i(-\frac{N}{2}+\frac{1}{2})x} - e^{i(\frac{N}{2}-\frac{1}{2})x}}{e^{-i\frac{x}{2}} - e^{i\frac{x}{2}}} = \frac{\sin(\frac{N-1}{2}x)}{\sin\frac{x}{2}}$$

This expression can be differentiated to yield the desired sum,

$$\frac{dS}{dx} = \sum_{k=\frac{N}{2}+1}^{\frac{N}{2}-1} ike^{ikx}$$

$$= \frac{\frac{N-1}{2}\cos(\frac{N-1}{2}x)\sin(\frac{x}{2}) - \frac{1}{2}\cos(\frac{x}{2})\sin(\frac{N-1}{2}x)}{(\sin\frac{x}{2})^2}$$

This expression can be simplified using trigonometric identities and noting that $x = \frac{2\pi}{N}(n-j)$:

$$\sin(\frac{N-1}{2}x) = \sin(\frac{N}{2}x - \frac{x}{2}) = -(-1)^{n-j}\sin(\frac{x}{2})$$

$$\cos(\frac{N-1}{2}x) = \cos(\frac{N}{2}x - \frac{x}{2}) = (-1)^{n-j}\cos(\frac{x}{2})$$

Therefore

$$\frac{dS}{dx} = \frac{\frac{N-1}{2}(-1)^{n-j}\cos(\frac{x}{2})\sin(\frac{x}{2}) + \frac{1}{2}(-1)^{n-j}\sin(\frac{x}{2})\cos(\frac{x}{2})}{(\sin\frac{x}{2})^2}$$

Thus:

$$d_n^j = \begin{cases} \frac{1}{2}(-1)^{n-j}\cot(\frac{\pi(n-j)}{N}) & : n \neq j \\ 0 & : n = j \end{cases}$$

2) A.2 Odd Formulation

For Odd Formulation, same calculation has been done. Finally:

$$d_n^j = \begin{cases} \frac{1}{2}(-1)^{n-j}\operatorname{cosec}(\frac{\pi(n-j)}{N}) & : n \neq j \\ 0 & : n = j \end{cases}$$

REFERENCES

[1] K.C. Hall, J.P. Thomas and W.S. Clark, "Computation of Unsteady Nonlinear Flows in Cascades using a Harmonic Balance Technique," Technical report, *9th International Symposium on Unsteady Aerodynamics, Aeroacoustics and Aeroelasticity Of Turbomachines*, Lyon, France, September 2000.

[2] M. McMullen, A. Jameson and J. J. Alonso, "Application of a Nonlinear Frequency Domain Solver to the Euler and Navier- Stokes Equations," AIAA paper 02-0120, *AIAA 40th Aerospace Sciences Meeting and Exhibit*, Reno, NV, January 2002,

[3] A. K. Gopinath and A. Jameson, "Time Spectral Method for Periodic Unsteady Computations over Two- and Three- Dimensional Bodies," *In AIAA 43th Aerospace Sciences Meeting & Exhibit* . Reno, NV, AIAA Paper 2005–1220.

[4] S.S. Davis, "NACA 64A010 (NASA Ames Model) Oscillatory Pitching ," *AGARD Report 702*, AGARD, January 1982, Dataset 2.

[5] R.H. Landon., "NACA0012 Oscillatory and Transient Pitching," *AGARD Report 702*, AGARD, January 1982. Dataset 3.

[6] A. Jameson, W. Schmidt and E. Turkel, "Numerical solutions of the Euler equations by finite volume methods with Runge-Kutta time stepping schemes," *AIAA paper 81-1259*, January 1981.

[7] Baldwin, B. S. and Lomax H., "Thin layer approximation and algebraic model for separated flows," *AIAA paper 78-275*, 1978.

[8] P. Moin, "*Spectral Methods in Computational Physics*, Supplementary notes," Stanford University, Stanford, CA, ME 408, 2003.